THE JOURNAL OF PHYSICAL CHEMISTRY C
A JOURNAL OF THE AMERICAN CHEMICAL SOCIETY

pubs.acs.org/JPCC
Article

Assessing Ni_2(dobpdc) Anchoring for Mitigating Lithium Polysulfide Dissolution in Lithium−Sulfur Batteries

Kuan-Yu Lin, Mei-Ru Lai, Minoru Otani, Tsuyoshi Miyazaki,* and Jyh-Chiang Jiang*

Cite This: J. Phys. Chem. C 2024, 128, 16334−16342
Read Online

ACCESS | Metrics & More | Article Recommendations | Supporting Information

ABSTRACT: In this work, we have explored sulfur loading, the anchoring ability of lithium polysulfides (LiPSs), and the formation mechanism of a net-like Li_2S structure in a Ni_2(dobpdc) metal−organic framework (MOF) using density functional theory (DFT) calculations and molecular dynamics (MD) simulations. The MD results reveal a net-like structure of $(Li_2S)_n$ covering the Ni_2(dobpdc) MOF surface when the S_8 cluster is transformed into short-chain LiPS molecules at a high level of lithiation. Further, the LiPS molecules adsorbed on the Ni_2(dobpdc) MOF surface (in the presence of a solvent) have been considered. Based on the electron distribution analysis of the three-dimensional reference interaction site model (3D-RISM) results, 1,3-dioxolane (DOL) can hinder LiPS dissolution owing to its weak binding strength with the LiPS molecules. In contrast, the ethylene carbonate (EC) solvent significantly decreases the adsorption strength of the long-chain LiPS molecules, leading to a severe shuttling effect of the LiPSs in Ni_2(dobpdc). Our findings indicate that the shuttling effect of the LiPSs is highly dependent on the dielectric constant of solvents, suggesting that solvents with a strong polarizability, such as EC, should be avoided. The present findings also offer comprehensive insights into the impact of various solvents on LiPS adsorption in Ni_2(dobpdc), paving the way for developing innovative cathode materials for next-generation Li−S batteries.

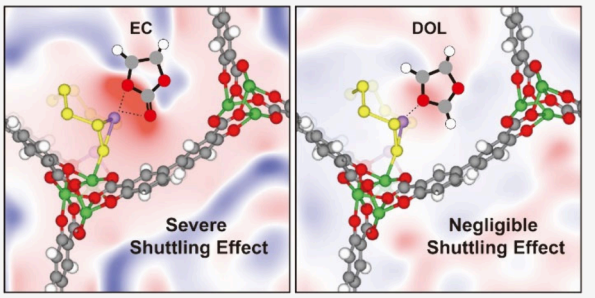

1. INTRODUCTION

In recent decades, there has been extensive research on high-energy-density lithium-ion batteries (LIBs) due to the growing demand for electronic devices and electric vehicles.[1−3] LIBs have emerged as a primary power source, widely used in various applications. Therefore, further development of high-energy-density LIBs has attracted considerable attention. However, because of intercalation during the lithiation and delithiation processes, most cathode materials begin to degrade, limiting the applications of LIBs because their structural stability becomes very unstable. Therefore, different battery systems have been explored to improve the energy density and capacity of LIBs, with several significant results achieved, such as lithium−sulfur (Li−S) batteries.[4−6] Li−S batteries have garnered extensive research interest owing to their environmental sustainability, natural abundance of S, low fabrication cost, and ultrahigh theoretical capacity of 1675 (mA h)/g.[7] However, the commercialization of Li−S batteries is still hindered by several intrinsic issues, including (1) the capacity of Li−S batteries lagging far behind the theoretical capacity due to the insulating characteristic of an S_8 cluster and its discharge products Li_2S and Li_2S_2 ($\sim 10^{-30}$ S/cm), (2) the occurrence of large volume change during the lithiation process, causing structural deformation of cathode materials and the poor stability of batteries, and (3) the dissolution of lithium polysulfides (LiPSs) causing a severe shuttle phenomenon, which leads to the corrosion of Li electrodes, severe loss in active electrode materials, and the rapid decay of batteries' capacity.[4−6,8−11] Therefore, it is necessary to design and develop innovative cathode materials that overcome these limitations.

Lately, considerable effort has been devoted to modifying cathode materials using physical confinement or chemical adsorption with porous conductive materials.[4,11−13] These conductive materials can effectively improve the electrical conductivity of S electrodes and reduce structural transformation during the charging and discharging processes, owing to their unique porous structure. However, the interaction between LiPSs and these carbon (C) materials remains very weak, causing a severe shuttling effect; hence, it is challenging to employ these conductive porous C materials as a cathode in Li−S batteries. Currently, black phosphorus,[14] polar metal compounds (carbides, oxides, nitrides, and sulfides),[15] MXenes,[16−18] and metal−organic framework materials (MOFs)[12,19−21] are widely employed in Li−S batteries. Among them, research on MOFs for Li−S battery

Received: May 13, 2024
Revised: September 11, 2024
Accepted: September 16, 2024
Published: September 20, 2024

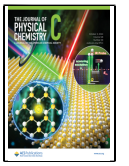

https://doi.org/10.1021/acs.jpcc.4c03165
J. Phys. Chem. C 2024, 128, 16334−16342

applications has increased considerably, with the trend continuing to grow, reflecting the great potential of MOFs in the field of Li−S batteries.[19] Tarascon et al. reported the use of a MIL-100(Cr)-based composite as a cathode material in Li−S batteries.[22] Subsequently, various MOFs were extensively investigated, such as ZIF-8, MIL-53(Al), and HKUST-1-based cathodes. The studies showed that MOF-based cathode materials can achieve a high number of cycles and excellent capacity retention during the charging and discharging process.[23] Wu et al. showed that ZIF-8 combined with carbon nanotubes successfully confined polysulfides within the cathode region, significantly improving the reversible capacity and cycling stability.[24]

Apart from functionalized ZIF-8 materials, M_2(dobdc) and its derivative M_2(dobpdc) have also been considered as potential cathode materials due to their high density of open metal sites when compared to all other known MOF materials, providing an abundance of active adsorption sites for anchoring sulfur and lithium polysulfide molecules.[25−27] The wealth of active adsorption sites for sulfur adsorption also endows M_2(dobdc) and M_2(dobpdc) MOF with a high sulfur loading capacity, making it a desirable cathode material. Furthermore, M_2(dobpdc) is constructed from unsaturated metal $(M)^{2+}$ ions and 4,4′-dioxidobiphenyl-3,3′-dicarboxylate (dobpdc) linkers, resulting in a distinctive one-dimensional (1-D) closely packed structure. This 1-D channel greatly enhances lithium accessibility to M_2(dobpdc) MOF with minimal tortuosity. In addition, the 1-D channel can significantly enhance the electrical conductivity of the MOF, thereby increasing sulfur conversion kinetics and exhibiting good charge storage capacity.[28−30] Finally, M_2(dobpdc) MOF is characterized by its substantial surface area, exceeding 1000 m^2/g, making it an excellent candidate as a sulfur host material for Li−S batteries.[31,32] In addition, Zheng et al. showed that Nickel (Ni)-MOF as a S host can provide physical confinement and chemical interaction to capture LiPSs, greatly improving the cycling stability and capacity retention of Li−S batteries.[33] Li et al. also demonstrated that highly mesoporous N-rich C with single Ni sites enables the effective confinement of LiPSs.[34] To gain a comprehensive understanding of the roles played by unsaturated metal Ni^{2+} ions and the functional group of dobpdc linkers on the behavior of LiPSs and to reveal how solvent properties affect the anchoring capabilities of Ni_2(dobpdc) MOF, Ni_2(dobpdc) MOF was adopted as the cathode material and the function of the unsaturated Ni^{2+} center of the MOF on the adsorption of LiPSs was computationally investigated via density functional theory (DFT) calculations. Furthermore, the reactivity of various solvents against the anchoring ability of the Ni_2(dobpdc) MOF was evaluated using three-dimensional (3-D) reference interaction site model (3D-RISM) simulations. The present study considered commercial solvents, such as ethylene carbonate (EC), dimethyl carbonate (DMC), dimethyl sulfoxide (DMSO), and 1,3-dioxolane (DOL). In addition to studying the anchoring ability of the Ni_2(dobpdc) MOF and the solvent effects on LiPS adsorption, lithiation of the S_8 cluster during the discharging process in Li−S batteries was also examined. This study conducted ab initio molecular dynamics (AIMD) simulations to formulate a detailed lithiation mechanism of Li_2S and Li_2S_2 formation in the Ni_2(dobpdc) MOF. With a deeper understanding of Ni_2(dobpdc) MOF and its interaction with various solvents affecting LiPS dissolution, the authors believe that this study could provide new insight into developing of innovative cathode materials for Li−S batteries.

2. COMPUTATIONAL METHODS

In this study, the optimized configurations of the Ni_2(dobpdc) MOF and analyses of the adsorption energies were performed using DFT within the plane-wave basis set approach.[35] All spin-polarized DFT calculations were performed using the Vienna Ab initio Simulation Package (VASP) with the projector-augmented wave method.[36,37] The generalized gradient approximation and long-range dispersion correction incorporated into the PBE-D2 functional were adopted to describe van der Waals interactions.[38,39] A cutoff energy of 550 eV was used for the structural optimization, electronic property analysis, and AIMD simulations. The gamma point was considered for Brillouin zone integration. The Hubbard U corrections of 5.96 were considered to include the self-interaction energy of the correlated d-electrons of Ni atoms in the system.[40,41] For the structural configuration relaxation, all geometrical parameters were relaxed until the total energy and Hellmann−Feynman forces on each atom converged to 10^{-5} eV and 0.01 eV/Å, respectively. The average adsorption energy of S_8 molecules (E_{ads}) on the Ni_2(dobpdc) MOF surface was calculated as in eq 1

$$E_{ads} = (E_{Total} - E_{Ni_2(dobpdc)} - nE_{S_8})/n \quad (1)$$

where E_{Total}, $E_{Ni_2(dobpdc)}$, and E_{S_8} are the total energies of the S_8 molecule adsorption on the Ni_2(dobpdc) MOF surface, pristine Ni_2(dobpdc) MOF structure, and isolated S_8 molecules, respectively. A label (n) was used to indicate the number of adsorbed S_8 molecules in Ni_2(dobpdc) MOF. In addition, the stepwise energy (E_{step}) of the adsorption of the S_8 molecules was considered by eq 2:

$$E_{step} = E_{Total}(nS_8) - E_{Total}((n-1)S_8) \quad (2)$$

For AIMD simulations, the convergence criteria for electronic self-consistent iteration were set to 10^{-4}. To simulate the lithiation process, step-by-step lithiation was performed on the Ni_2(dobpdc) MOF surface. Five stages of the lithiation process were considered, wherein one, three, four, four, and four Li atoms were added to the system at different stages. After adding Li atoms, the AIMD simulations were equilibrated at 300 K in a canonical ensemble (NVT) for a total time of 5 ps (with a time interval of 1 fs).

To investigate the solvent effects of LiPS adsorption on the Ni_2(dobpdc) MOF surface, the 3D-RISM was used for further calculations.[42,43] The 3D-RISM calculations provide the solvent structure in the form of a 3D site distribution function and enable the calculations of structural optimization, electronic properties, and molecular solvation structure in each molecular liquid or mixture. Compared with other implicit solvation models, the 3D-RISM method provides more detailed information about solvent effects, such as the solvent density distribution and charge density surrounding the solute. The method also possesses significant advantages over explicit solvation models in terms of computational efficiency and cost. As 3D-RISM was not implemented in the VASP software, all calculations in the presence of implicit solvation models were performed using the Quantum ESPRESSO code.[44,45] All spin-polarized calculations were performed with plane-wave basis sets and ultrasoft pseudopotentials.[46,47] For structural optimization in the presence of solvent effects, all geometrical

https://doi.org/10.1021/acs.jpcc.4c03165
J. Phys. Chem. C 2024, 128, 16334−16342

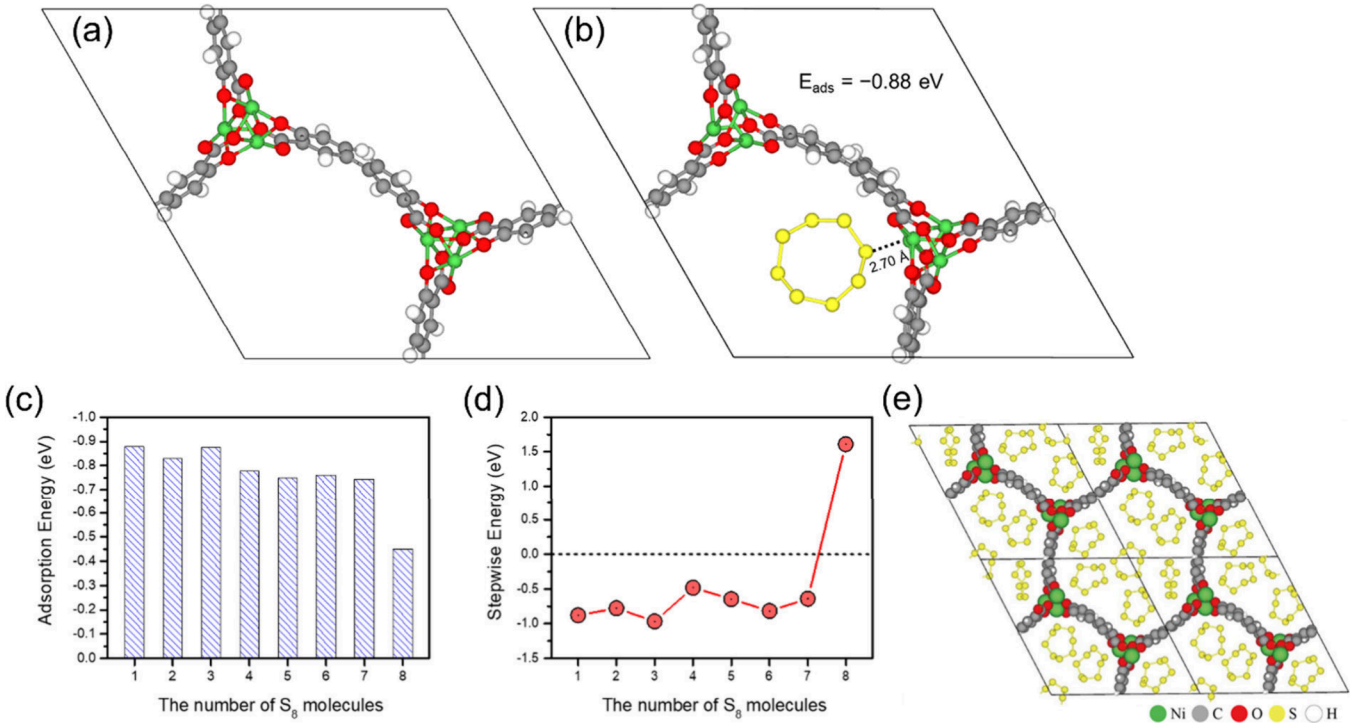

Figure 1. (a) The optimized structure of the unit cell of Ni_2(dobpdc). (b) The most stable adsorption configuration of S_8 molecule with Ni_2(dobpdc). Calculated (c) average adsorption energy and (d) Stepwise adsorption energy of S_8 clusters in the Ni_2(dobpdc) MOF. (e) Illustration of the maximum sulfur loading in the $p(4 \times 1)$ supercell of Ni_2(dobpdc).

parameters were relaxed until the total energy converged to 10^{-4} (Ry) and the forces on each atom were smaller than 10^{-3} (Ry/Bohr). For the 3D-RISM calculations, the LJ parameters were obtained from the table of the nonbonded OPLS−AA force fields.[48] The convergence criterion for the root-mean-square of the residual of the total correlation function in the MDIIS iteration was 10^{-7} (Bohr). This study considered the solvent concentrations for EC, DMC, DMSO, and DOL to be 1.32, 1.07, 1.10, and 1.06 g/cm^3, respectively.

3. RESULTS AND DISCUSSION

3.1. Sulfur Loading and Theoretical Capacity of Ni_2(dobpdc). Ni_2(dobpdc) was composed of inorganic nodes (Ni^{2+}) and organic linkers (dobpdc^{-4}). The unsaturated Ni^{2+} center in Ni_2(dobpdc) was demonstrated by bonding each Ni^{2+} ion to five oxygen atoms. Beginning from the hexagonal unit cell of Ni_2(dobpdc) with periodic boundary conditions, a unit cell containing a 6 Ni^{2+} center was considered to study the interaction of the unsaturated metal site with S_8 molecules, as shown in Figure 1a. To understand the adsorption behavior of the S_8 molecule on Ni_2(dobpdc), we have examined the adsorption of a S_8 molecule at all possible adsorption sites, including directly on top of the Ni^{2+} cation, O^{2-} anion, and above the center of the organic linker. Figure 1b illustrates the most stable configuration of S_8 molecule adsorption on Ni_2(dobpdc). We found that the S_8 molecule could be stably adsorbed on the top of the Ni^{2+} cation, with an adsorption energy of −0.88 eV. The distance between the S atom and Ni^{2+} cation is 2.70 Å. To explore the behavior of multiple adsorptions and its impact on the sulfur capacity retention of Ni_2(dobpdc), we gradually added additional S_8 molecules to the other Ni^{2+} cation sites. After each addition, the system was reoptimized to determine the most stable configuration. We continued this process until the stepwise adsorption energy for the nth S_8 molecule became positive. The average adsorption energy and stepwise energy were calculated and illustrated in Figure 1(c,d). The corresponding geometries of the adsorbed S_8 in Ni_2(dobpdc) are shown in the Supporting Information (Figure S1). Figure 1c demonstrates that the calculated average S_8 adsorption energies range from −0.88 to −0.74 eV as the amount of adsorbed S_8 molecules varied from 1 to 7. Among them, the first S_8 molecule demonstrates the largest adsorption strength of −0.88 eV. As the number of adsorbed S_8 molecules increases to seven, the adsorption energy remains relatively constant. Nevertheless, the S_8 adsorption energy decreased significantly when more than one S_8 molecule was adsorbed. Figure 1d shows that the stepwise adsorption energy of the eighth S_8 molecule becomes positive (1.61 eV), indicating that its adsorption is thermodynamically unfavorable. The calculations revealed that seven S_8 molecules can stably adsorb onto the Ni_2(dobpdc) MOF, as shown in Figure 1e. In an ideally completed electrochemical reaction for the formation of the final lithiated product (Li_2S) during the discharging process, the final reaction product comprised 56 Li_2S molecules in the Ni_2(dobpdc) MOF. The theoretical capacity (C; mAh/g) of the electrode material was calculated using the formula C = NF/3.6m.[49] This formula considers the mole number of electron transfers (N) in the reaction, the Faraday constant (F = 96485 C/mol), and the mole mass of the electrode material (m). Based on the calculations, Ni_2(dobpdc) MOF, which contains seven S_8 clusters, has a theoretical capacity of 1016.3 mAh/g. In addition, we have examined the structural stability of Ni_2(dobpdc) as the number of S_8 molecules increases. The percentage volume change of Ni_2(dobpdc) is summarized in Figure S2. It can be clearly seen that the Ni_2(dobpdc) MOF exhibits excellent structural stability, with volume changes

https://doi.org/10.1021/acs.jpcc.4c03165
J. Phys. Chem. C 2024, 128, 16334−16342

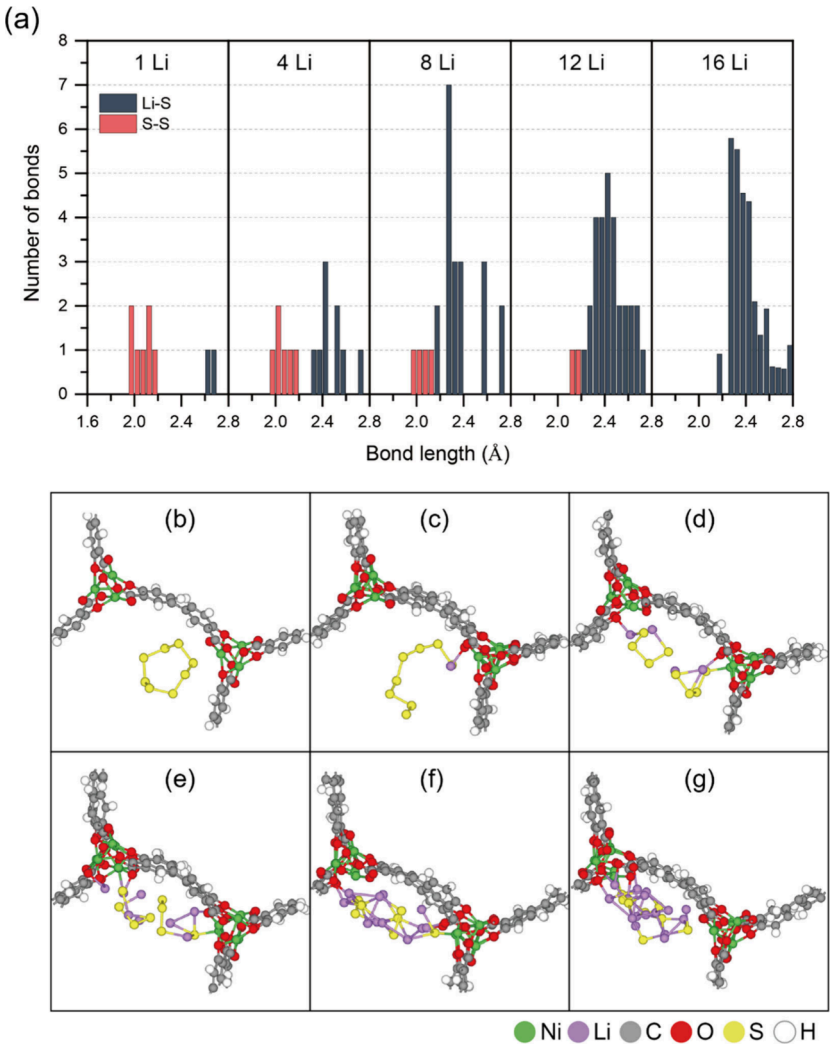

Figure 2. (a) Number of S−S bonds in S_8 molecules and that of Li−S formation at the different levels of lithiation. Snapshots of lithiation process of S_8 to $Li_{16}S_8$: (a) S_8, (b) LiS_8, (c) Li_4S_8, (d) Li_8S_8, (e) $Li_{12}S_8$, and (f) $Li_{16}S_8$.

smaller than ±2% after the insertion of S_8 molecules. Therefore, the high theoretical capacity and strong structural stability of the Ni_2(dobpdc) MOF might make it an effective host for capturing S_8 clusters, which could be applied to conventional Li−S batteries.

3.2. Sulfur Reduction Reaction in Ni_2(dobpdc). To further elucidate the S reduction reaction on the Ni_2(dobpdc) MOF surface during the discharging process in Li−S batteries, we examined the overall reaction from the S_8 molecule to the lithiated product of Li_2S using AIMD simulations. The overall simulation comprised five steps to model the lithiation process. A stepwise lithiation process was performed on Ni_2(dobpdc) by adding Li atoms at each step. After adding Li atoms to Ni_2(dobpdc), the system equilibrated for 5 ps, demonstrating a structural change and reaching a new equilibrium. In these five-step AIMD simulations, one, three, four, four, and four Li atoms were gradually added to the Ni_2(dobpdc) system. At the beginning of the AIMD simulation, we added a Li atom around the adsorbed S_8 molecule, and each subsequent addition of Li atoms was strategically positioned near the emerging LiPS structure formed in the previous step to facilitate the continuous lithiation process. The calculated total energy (in eV) of the system as a function of simulation time (in ps) after lithiation is illustrated in Figure S3. In addition, this study analyzed the number of S−S bond breaks in the S_8 molecules and the Li−S bond formation during the lithiation process, as shown in Figure 2a. With the addition of Li atoms, it can be observed that the number of S−S bonds decreased and that of Li−S bonds increased. In the presence of 16 Li atoms, the S−S bonds completely dissociated, and all S atoms combined with the Li atoms to form Li_2S. Furthermore, it was observed that when one Li atom was added to the system, the Li−S bond distances were between 2.6 and 2.7 Å. Nevertheless, when more Li atoms were added, the range of the Li−S bond distances widened, with most of the distances falling between 2.3 and 2.4 Å.

To perform a deeper analysis of the S−S bond breaking and Li−S bond formation, this study has depicted the configurations of the LiPS molecules adsorbed on the surface of the Ni_2(dobpdc) MOF, ranging from the lithiation level of S_8 to $Li_{16}S_8$. These illustrations are shown in Figure 2(b−g). Before the lithiation process, the S_8 molecule was adsorbed on the Ni_2(dobpdc) MOF surface and exhibited a ring structure with eight S−S bonds, as shown in Figure 2b. The first step involved the introduction of one Li atom into the system, which formed the LiPS structure of the adsorbed LiS_8. It was observed that one S−S bond broke and one Li−S bond formed, with the S_8 becoming a chain-like structure, as shown in Figure 2c. As

https://doi.org/10.1021/acs.jpcc.4c03165
J. Phys. Chem. C 2024, 128, 16334−16342

three extra Li atoms were added in the second step, the S_8 ring structure broke down, and the S_8 cluster began to decompose into two smaller Li_2S_4 species. When the lithiation level of the Li atoms reached 8 and 12, Li_2S_3 and Li_2S_2 were observed in the Ni_2(dobpdc) MOF system, respectively. In addition, the adsorbed LiPS molecules began to connect with each other, forming chain-like or net-like configurations. At the end of the lithiation process, when 16 Li atoms were added, there were no S−S bonds in the system, and all S atoms of the S_8 molecule were transformed into Li_2S molecules. Figure 2g demonstrates that all the Li_2S molecules are connected, forming net-like configurations and covering the Ni_2(dobpdc) MOF surface. In addition, the detailed mechanism of the S_8 reduction reaction on the Ni_2(dobpdc) MOF surface during lithiation are provided in Figure S4. The MD simulation results indicate that longer chain LiPS molecules are favorably transformed into short-chain LiPS molecules, which are further reduced to a net-like structure of $(Li_2S)_n$, covering the Ni_2(dobpdc) MOF surface.

3.3. Anchoring Ability of Ni_2(dobpdc). An ideal cathode material must have good anchoring properties toward LiPSs to inhibit the dissolution of the active materials. To evaluate the anchoring properties of Ni_2(dobpdc) as a potential cathode material, we optimized the structure of the LiPS molecules (Li_2S_x, x = 1−8) and calculated their adsorption energies (E_{ads}) on the Ni_2(dobpdc) MOF surface. The optimized structures of adsorbed Li_2S_x (x = 1−8) molecules on Ni_2(dobpdc) are shown in Figure 3. The Li atoms of all the LiPS molecules were

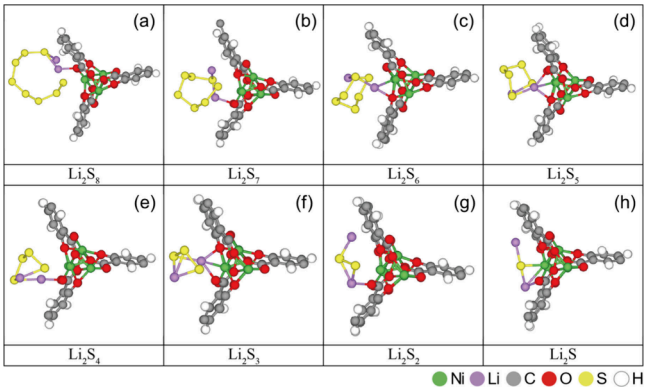

Figure 3. Optimized adsorption structures of Li_2S_x (x = 1−8) molecules on the Ni_2(dobpdc) MOF surface.

closer to the O atom of the organic linker, and the S atom was absorbed on top of the Ni atom. In addition, the formation of chemical bonds (Li−O) can be observed when all the LiPS molecules are adsorbed on the Ni_2(dobpdc) MOF surface, implying the strong anchoring ability of Ni_2(dobpdc) toward LiPSs. Table 1 lists the calculated E_{ads} values and the shortest adsorption distance of Li_2S_x to the central metal site (d_{S-Ni}) and the O atom of the organic linker (d_{Li-O}) for the most stable adsorption configurations. The calculation results indicate that the LiPS molecules can stably adsorb on the Ni_2(dobpdc), with the calculated adsorption energies ranging from −1.70 to −2.96 eV. As shown in Table 1, the Li_2S molecule demonstrated the strongest adsorption on the Ni_2(dobpdc) MOF surface, with the shortest S−Ni and Li−O distances of 2.33 and 1.86 Å, respectively, suggesting strong interactions between Li_2S and the Ni_2(dobpdc) MOF surface.

Table 1. Calculated Adsorption Energy (E_{ads}) Values and the Shortest Adsorption Distance of Li_2S_x to the Central Metal Site (d_{S-Ni}) and the O Atom of the Organic Linker (d_{Li-O}) for the Most Stable LiPS Adsorption Configurations

Clusters	E_{ads} (eV)	d_{S-Ni} (Å)	d_{Li-O} (Å)
Li_2S	−2.96	2.33	1.86
Li_2S_2	−2.43	2.39	1.92
Li_2S_3	−1.91	2.43	1.98
Li_2S_4	−1.70	2.47	1.86
Li_2S_5	−1.88	2.46	1.98
Li_2S_6	−1.73	2.50	2.02
Li_2S_7	−1.98	2.43	1.89
Li_2S_8	−2.00	2.45	1.94
S_8	−0.88	2.70	-

Furthermore, the electron density difference (EDD) of the S_8 cluster and Li_2S molecule adsorption was systematically compared to identify the underlying cause of strong Li_2S adsorption on the Ni_2(dobpdc) MOF surface. The EDD results for S_8 and Li_2S adsorption on the Ni_2(dobpdc) MOF surface are illustrated in Figure 4, where the yellow region and

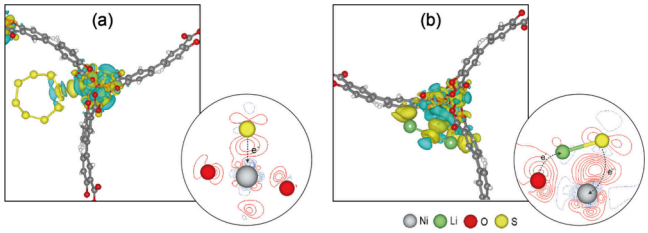

Figure 4. Illustrations of 3-D and 2-D electron density difference (EDD) of the Ni_2(dobpdc) MOF structure by the adsorption of (a) S_8 cluster and (b) Li_2S molecule. The isosurface value is 0.001 e/au.

red line represent electron-rich areas, and the blue region and blue line indicate electron-deficient areas. Figure 4a demonstrates a small accumulation of electrons between the adsorbed S_8 molecule and the Ni_2(dobpdc) MOF surface, indicating that S_8 molecule adsorption on the surface occurs via the dative bond, and the electrons are transferred from the S atom to the Ni atom. In contrast, the electron difference between the adsorbed Li_2S and Ni_2(dobpdc) MOF surfaces (Figure 4b) was enormous, which shows an increased adsorption strength. To further understand the interaction between the adsorbed Li_2S and Ni_2(dobpdc) MOF surface, the two-dimensional (2-D) EDD of Li_2S adsorption was analyzed. The electron density (red line) increased between the O−Li and S−Ni bonds; this observed increase demonstrates the presence of a dative bond between O and Li and between S and Ni, suggesting that electrons are transferred from O to the Li cation and from S to the Ni cation. This electron transfer direction results in a cooperative effect of the two interactions, increasing the interaction energy between the Li_2S molecule and the Ni_2(dobpdc) MOF. Therefore, these results suggest that the cooperative binding of LiPS molecules provides the Ni_2(dobpdc) MOF with a stronger anchoring ability to store LiPS molecules.

Based on the findings above, the Ni atom in the Ni_2(dobpdc) MOF plays a significant role in improving the capacity retention of Li_2S. Besides enhancing the capacity of Li_2S, the oxidation state changes of Ni atoms during lithiation can also affect the stability of the Ni_2(dobpdc) MOF. It has

https://doi.org/10.1021/acs.jpcc.4c03165
J. Phys. Chem. C 2024, 128, 16334−16342

been reported that changes in the magnetic moment from Ni^{2+} to Ni^{3+} in Ni-based cathode materials can induce Jahn−Teller distortion, leading to structural instability.[50,51] Consequently, we examined the magnetic moments of the Ni ions both before and after Li_2S adsorption, as shown in Table 2. Our

Table 2. Calculated Magnetic Moments for Ni Ions in Pristine and Li_2S-Adsorbed Ni_2(dobpdc)

	Magnetic moment (μ_B)		
	Pristine Ni_2(dobpdc)	Li_2S adsorption on Ni_2(dobpdc)	
Ni ions	(Figure 1a)	1Li_2S (Figure 2g)	Net-like Li_2S (Figure 3h)
Ni (1)	1.805	1.771	1.807
Ni (2)	1.805	1.806	1.807
Ni (3)	1.805	1.804	1.809
Ni (4)	1.808	1.801	1.806
Ni (5)	1.807	1.811	1.807
Ni (6)	1.807	1.808	1.807
Ni (7)	1.805	1.749	1.762
Ni (8)	1.805	1.817	1.810
Ni (9)	1.806	1.799	1.812
Ni (10)	1.806	1.810	1.806
Ni (11)	1.805	1.803	1.807
Ni (12)	1.806	1.804	1.807

calculations reveal that the magnetic moment of Ni ions before Li_2S adsorption is approximately 1.8 μ_B, while it slightly decreases to around 1.77 μ_B after Li_2S adsorption. Previous studies have shown that Ni ions exhibit a magnetic moment of approximately 1.7 μ_B in their +2 oxidation state and around 1.1 μ_B in their +3 state.[50] Therefore, our findings indicate that there is no Jahn−Teller distortion following Li_2S adsorption.

3.4. Solvent Effects on the Anchoring Ability. Li−S batteries are known to suffer from the "shuttling effect", which is caused by poor anchoring of the discharge product (LiPS) over the cathode material. One of the key factors influencing the adsorption strength of LiPS molecules and their subsequent dissolution is the solvent used. To investigate this, this study used the 3D-RISM solvation method to study solvent effects on the binding ability of Ni_2(dobpdc) toward LiPS molecules. The adsorption energies (E_{ads}) in both vacuum and solvents were calculated. For a more comprehensive discussion of the solvent effects on the LiPS adsorption on Ni_2(dobpdc), four common solvents were selected: EC, EMC, DMSO, and DOL. The calculated adsorption energies (E_{ads}) of Li_2S_n (n = 1, 2, 4, 6, and 8) on the Ni_2(dobpdc) MOF surfaces in each solvent are shown in Figure 5. The calculated adsorption energies for all the LiPS molecules are listed in Table S1. The EC solvent exhibits a significant influence on LiPS adsorption, particularly for the long-chain Li_2S_8, Li_2S_6, and Li_2S_4. The calculated value of the adsorption energy of Li_2S_8 in EC becomes positive, implying that Li_2S_8 adsorption on the Ni_2(dobpdc) MOF surface is thermodynamically unfavorable. In other words, long-chain Li_2S_8 molecules dissolve easily in the EC solvent. In addition, DMSO also demonstrated weak adsorption strength of long-chain LiPS molecules, suggesting that EC and DMSO should be avoided as electrolyte solutions in experiments. However, the calculated adsorption energies of Li_2S_8 adsorption in the DMC and DOL solvents were −0.85 and −1.05 eV, respectively, showing that

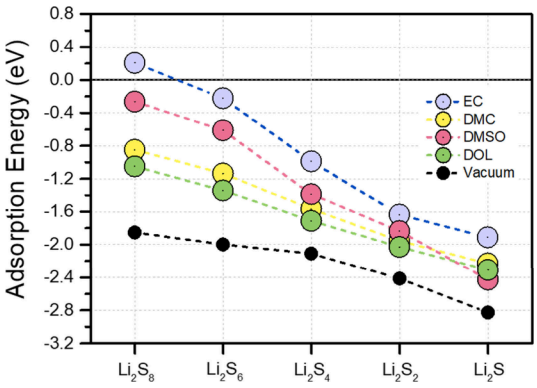

Figure 5. Calculated adsorption energies of Li_2S_8, Li_2S_6, Li_2S_4, Li_2S_2, and Li_2S molecules on the Ni_2(dobpdc) MOF surface in the presence of 3D-RISM solvation models, which include EC, DMC, DMSO, and DOL solvents.

the Ni_2(dobpdc) MOF can hinder the shuttling effect and could be applied to either the DMC or DOL solvents.

The 2-D charge density distribution of the solvent was analyzed using 3-D RISM calculations to discern the influence of each solvent on the adsorption of LiPS on the Ni_2(dobpdc) MOF surface. The obtained 2-D charge density distribution plot obtained for each solvent is shown in Figure 6, wherein the red and blue areas represent the increase and decrease of the charge density distribution, respectively. In the EC solvent system, the charge density is significantly increased near the Li atom of the Li_2S_8 molecule. This reveals a strengthening of the electrostatic interaction between the adsorbed Li_2S_8 molecule and the implicit EC solvent, confirming that the strong interaction decreases the adsorption strength of long-chain Li_2S_8 on the Ni_2(dobpdc) MOF surface. In contrast, in the DOL solvent system, the charge density near the Li atom is very small, which implies a weak interaction between Li_2S_8 and the DOL solvent and the strong adsorption of the long-chain Li_2S_8 on the Ni_2(dobpdc) MOF surface. Based on the analyses of charge density in the surroundings of the Li atom shown in Figure 6, the results support that the solvent effect on the adsorption strength of the adsorbed Li_2S_8 molecules from strong to weak is EC, DMSO, DMC, and DOL. To gain insight into the interactions between the long-chain Li_2S_8 molecules and various solvents, the 1-D projector of the charge density distribution was analyzed along the z-axis, as shown in Figure S5. The dielectric constant, the highest charge density of the 1-D projector, the solvation free energies, and the adsorption energies of the Li_2S_8 molecules in each solvent system are summarized in Table 3. The low dielectric constant might have caused an decreased charge density of the implicit solvent, resulting in weak electrostatic interactions between the Li_2S_8 and solvent molecules. Thus, the weak interaction between the Li_2S_8 and solvent molecules leads to lower solvation free energy, making Li_2S_8 adsorption thermodynamically favorable. Therefore, this suggests that solvents with a low dielectric constant, such as DOL, are suitable for Li−S batteries because of their weak interactions with the LiPSs, thus suppressing the subsequent shuttling effect.

4. CONCLUSIONS

A Ni_2(dobpdc) MOF was systematically investigated as a Li−S battery cathode material using first-principles calculations, AIMD simulations, and 3D-RISM solvation models. By

https://doi.org/10.1021/acs.jpcc.4c03165
J. Phys. Chem. C 2024, 128, 16334−16342

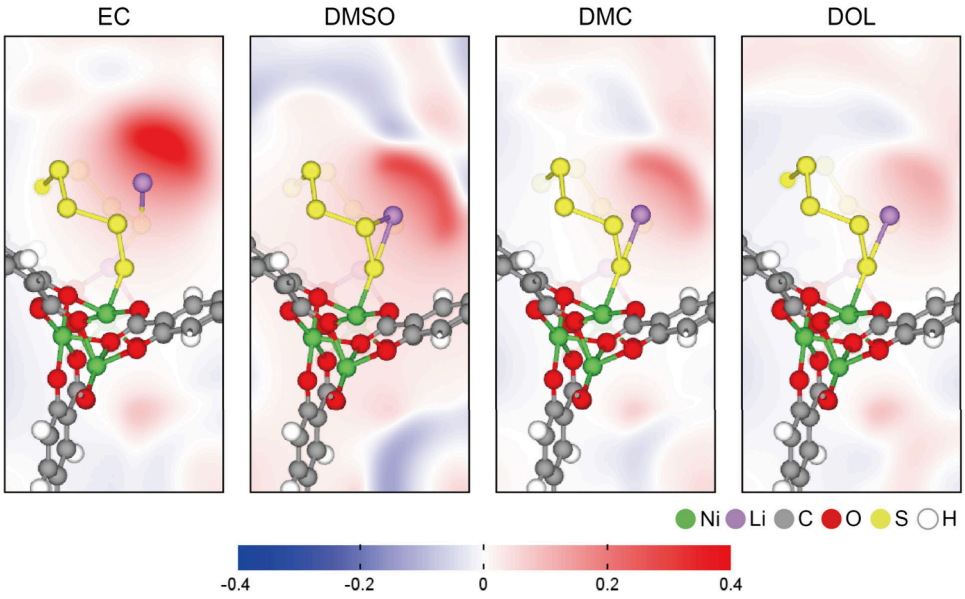

Figure 6. Charge density distributions of solvent molecules in relation to the adsorption of Li_2S_8 molecule on the Ni_2(dobpdc) MOF structure in the EC, DMSO, DMC, and DOL solvents.

Table 3. Dielectric Constant of Each Solvent, Highest Charge Density of the 1-D Projector, Calculated Solvation Free Energies, and Adsorption Energies of the Li_2S_8 Molecule in Each Solvent System

	Dielectric constant	Charge Density ($1/Bohr^3$)	Solvation Free Energy (eV)	Li_2S_8 Adsorption Energy (eV)
EC	89.6	0.22	2.63	0.21
DMSO	46.7	0.18	1.95	−0.26
DMC	3.11	0.13	1.61	−0.85
DOL	7.13	0.08	1.41	−1.05

identifying and analyzing the S_8 cluster adsorption on Ni_2(dobpdc), the adsorption and stepwise adsorption energies of the S_8 molecule were calculated. The results indicated that the Ni_2(dobpdc) MOF can store up to seven S_8 molecules with the largest average adsorption energy of −0.88 eV. The Ni_2(dobpdc) MOF showed high sulfur loading and a high theoretical capacity of 1016.3 mAh/g, suggesting that it could be used as a potential cathode material. In addition, the lithiation process in Ni_2(dobpdc) was considered using AIMD simulations, and it was observed that the S_8 cluster favorably transformed into short-chain LiPS molecules. A net-like structure of $(Li_2S)_n$ covering the Ni_2(dobpdc) MOF surface was perceived at high levels of lithiation. To further investigate the anchoring ability to capture lithiation products, we analyzed the adsorption of LiPS onto the Ni_2(dobpdc) surface. Based on the calculated results, all LiPSs can strongly interact with Ni_2(dobpdc) through the combination of S−Ni and Li−O covalent bonds, revealing the existence of cooperative interactions between LiPSs and the surface. Among all LiPS adsorption, the Ni_2(dobpdc) MOF exhibited the largest adsorption energy of −2.96 eV toward Li_2S adsorption. Furthermore, this study investigated the shuttling effect of LiPSs in Ni_2(dobpdc) using various solvent molecules. Analyses of the electron density distribution of each solvent from the 3-D solvation results revealed that many electrons accumulated near the Li atom of the adsorbed Li_2S_8 in the presence of the EC solvent. Such electron accumulation indicates a strong interaction between the adsorbed Li_2S_8 and EC molecules, making Li_2S_8 adsorption thermodynamically unfavorable. In contrast, less electron accumulation and weak interactions between the adsorbed Li_2S_8 and DOL molecules resulted in strong Li_2S_8 adsorption on the surface. This theoretical study indicates that that utilizing Ni_2(dobpdc) MOF with a low dielectric constant solvent, such as DOL, could be considered as a promising cathode material option due to its enhanced sulfur loading and outstanding performance in mitigating the shuttling effect.

■ ASSOCIATED CONTENT

Supporting Information

The Supporting Information is available free of charge at https://pubs.acs.org/doi/10.1021/acs.jpcc.4c03165.

The corresponding geometries of the adsorbed S_8 in Ni_2(dobpdc) and the calculated adsorption energies for all the LiPS molecules, the percentage volume change of Ni_2(dobpdc) after the insertion of S_8 molecules, the calculated total energy (in eV) of the system as a function of simulation time (in ps) after lithiation, the detailed mechanism of the S_8 reduction reaction on the Ni_2(dobpdc) MOF surface during lithiation, and the 1-D projector of the charge density distribution was analyzed along the *z*-axis (PDF)

■ AUTHOR INFORMATION

Corresponding Authors

Tsuyoshi Miyazaki − *Research Center for Materials Nanoarchitectonics (MANA), National Institute for Materials Science (NIMS), Tsukuba, Ibaraki 305-0044, Japan;* orcid.org/0000-0003-3534-4404; Email: miyazaki.tsuyoshi@nims.go.jp

Jyh-Chiang Jiang − *Department of Chemical Engineering, National Taiwan University of Science and Technology, Taipei City 106335, Taiwan;* orcid.org/0000-0002-4225-5250; Email: jcjiang@mail.ntust.edu.tw

https://doi.org/10.1021/acs.jpcc.4c03165
J. Phys. Chem. C 2024, 128, 16334−16342

Authors

Kuan-Yu Lin − *Department of Chemical Engineering, National Taiwan University of Science and Technology, Taipei City 106335, Taiwan; Research Center for Materials Nanoarchitectonics (MANA), National Institute for Materials Science (NIMS), Tsukuba, Ibaraki 305-0044, Japan;* orcid.org/0000-0002-2426-5543

Mei-Ru Lai − *Department of Chemical Engineering, National Taiwan University of Science and Technology, Taipei City 106335, Taiwan*

Minoru Otani − *Center for Computational Sciences, University of Tsukuba, Tsukuba, Ibaraki 305-8577, Japan*

Complete contact information is available at: https://pubs.acs.org/10.1021/acs.jpcc.4c03165

Notes

The authors declare no competing financial interest.

■ ACKNOWLEDGMENTS

All the authors gratefully acknowledge the financial support from the National Science and Technology Council (NSTC), Taiwan (110-2113-M-011-002-MY3, 110-2923-M-011-003-MY2, and 111-2926-I-011-501-G), and Sustainable Electrochemical Energy Development Center (SEED) supported by the Ministry of Education (MOE), Taiwan. The authors are also thankful to the National Center of High-Performance Computing (NCHC) for donating computer time and facilities. K.Y.L. and T.M. are supported by World Premier International Research Center Initiative (WPI), MEXT. Part of the calculations were performed on the Numerical Materials Simulator at NIMS.

■ REFERENCES

(1) Yu, W. H.; Guo, Y.; Xu, S. M.; Yang, Y.; Zhao, Y. F.; Zhang, J. J. Comprehensive recycling of lithium-ion batteries: Fundamentals, pretreatment, and perspectives. *Energy Storage Mater.* **2023**, *54*, 172−220.

(2) Ju, Z. Y.; Xu, X.; Zhang, X.; Raigama, K. U.; Yu, G. H. Towards fast-charging high-energy lithium-ion batteries: From nano- to micro-structuring perspectives. *Chem. Eng. J.* **2023**, *454*, No. 140003.

(3) Hu, X. Q.; Wang, C.; Lim, M. K.; Chen, W. Q.; Teng, L. M.; Wang, P.; Wang, H. M.; Zhang, C.; Yao, C. Y.; Ghadimi, P. Critical systemic risk sources in global lithium-ion battery supply networks: Static and dynamic network perspectives. *Renewable Sustainable Energy Rev.* **2023**, *173*, No. 113083.

(4) Chadha, U.; Bhardwaj, P.; Padmanaban, S.; Suneel, R. M.; Milton, K.; Subair, N.; Pandey, A.; Khanna, M.; Srivastava, D.; Mathew, R. M.; et al. Contemporary Progresses in Carbon-Based Electrode Material in Li-S Batteries. *J. Electrochem. Soc.* **2022**, *169*, No. 020530.

(5) Zhou, L.; Danilov, D. L.; Eichel, R. A.; Notten, P. H. L. Host Materials Anchoring Polysulfides in Li-S Batteries Reviewed. *Adv. Energy Mater.* **2021**, *11*, No. 2001304.

(6) Zhou, T.; Liang, J. N.; Ye, S. H.; Zhang, Q. L.; Liu, J. H. Fundamental, application and opportunities of single atom catalysts for Li-S batteries. *Energy Storage Mater.* **2023**, *55*, 322−355.

(7) Evers, S.; Nazar, L. F. New Approaches for High Energy Density Lithium−Sulfur Battery Cathodes. *Acc. Chem. Res.* **2013**, *46*, 1135−1143.

(8) Pang, Q.; Liang, X.; Kwok, C. Y.; Nazar, L. F. Advances in lithium-sulfur batteries based on multifunctional cathodes and electrolytes. *Nat. Energy* **2016**, *1*, 1−11.

(9) Manthiram, A.; Fu, Y.; Chung, S.-H.; Zu, C.; Su, Y.-S. Rechargeable Lithium−Sulfur Batteries. *Chem. Rev.* **2014**, *114*, 11751−11787.

(10) Raccichini, R.; Varzi, A.; Passerini, S.; Scrosati, B. The role of graphene for electrochemical energy storage. *Nat. Mater.* **2015**, *14*, 271−279.

(11) Chung, S.-H.; Chang, C.-H.; Manthiram, A. Progress on the Critical Parameters for Lithium−Sulfur Batteries to be Practically Viable. *Adv. Funct. Mater.* **2018**, *28*, No. 1801188.

(12) Lu, Y. Q.; Wu, Y. J.; Sheng, T.; Peng, X. X.; Gao, Z. G.; Zhang, S. J.; Deng, L.; Nie, R.; Swiatowska, J.; Li, J. T.; et al. Novel Sulfur Host Composed of Cobalt and Porous Graphitic Carbon Derived from MOFs for the High-Performance Li-S Battery. *ACS Appl. Mater. Interfaces* **2018**, *10*, 13499−13508.

(13) Perez Beltran, S.; Balbuena, P. B. A solid electrolyte interphase to protect the sulfurized polyacrylonitrile (SPAN) composite for Li-S batteries: computational approach addressing the electrolyte/SPAN interfacial reactivity. *J. Mater. Chem. A* **2021**, *9*, 7888−7902.

(14) Zhang, Q.; Xiao, Y. H.; Fu, Y. Y.; Li, C.; Zhang, X. F.; Yan, J.; Liu, J. Q.; Wu, Y. C. Theoretical prediction of B/Al-doped black phosphorus as potential cathode material in lithium-sulfur batteries. *Appl. Surf. Sci.* **2020**, *512*, No. 145639.

(15) Mei, J.; Liao, T.; Kou, L. Z.; Sun, Z. Q. Two-Dimensional Metal Oxide Nanomaterials for Next-Generation Rechargeable Batteries. *Adv. Mater.* **2017**, *29*, No. 1700176.

(16) Sim, E. S.; Yi, G. S.; Je, M. Y.; Lee, Y. B.; Chung, Y. C. Understanding the anchoring behavior of titanium carbide-based MXenes depending on the functional group in Li-S batteries: A density functional theory study. *J. Power Sources* **2017**, *342*, 64−69.

(17) Li, N.; Meng, Q. Q.; Zhu, X. H.; Li, Z.; Ma, J. L.; Huang, C. X.; Song, J.; Fan, J. Lattice constant-dependent anchoring effect of MXenes for lithium-sulfur (Li-S) batteries: a DFT study. *Nanoscale* **2019**, *11*, 8485−8493.

(18) Iqbal, N.; Ghani, U.; Liao, W.; He, X.; Lu, Y.; Wang, Z.; Li, T. Synergistically engineered 2D MXenes for metal-ion/Li-S batteries: Progress and outlook. *Mater. Today Adv.* **2022**, *16*, No. 100303.

(19) Ye, Z. Q.; Jiang, Y.; Li, L.; Wu, F.; Chen, R. J. Rational Design of MOF-Based Materials for Next-Generation Rechargeable Batteries. *Nanomicro Lett.* **2021**, *13*, 1−37.

(20) Fan, C. J.; Yang, R.; Liu, Y.; Chen, D.; Chen, L. P.; Liu, R.; Yan, Y. L.; Zou, Y. M.; Xu, Y. H. Alleviating the polysulfides "shuttling" and improving the sulfur utilization ably by the micropores of MOFs materials. *Int. J. Energy Res.* **2021**, *45*, 10304−10316.

(21) Qian, X. Y.; Wang, Y. H.; Jin, L. N.; Cheng, J.; Chen, J. Y.; Huang, B. B. Application of Ni-MOF derived Ni-C composite on separator modification for Li-S batteries. *J. Electroanal. Chem.* **2022**, *907*, No. 116029.

(22) Demir-Cakan, R.; Morcrette, M.; Nouar, F.; Davoisne, C.; Devic, T.; Gonbeau, D.; Dominko, R.; Serre, C.; Ferey, G.; Tarascon, J. M. Cathode Composites for Li-S Batteries via the Use of Oxygenated Porous Architectures. *J. Am. Chem. Soc.* **2011**, *133*, 16154−16160.

(23) Zhou, J. W.; Li, R.; Fan, X. X.; Chen, Y. F.; Han, R. D.; Li, W.; Zheng, J.; Wang, B.; Li, X. G. Rational design of a metal-organic framework host for sulfur storage in fast, long-cycle Li-S batteries. *Energy Environ. Sci.* **2014**, *7*, 2715−2724.

(24) Wu, F.; Zhao, S. Y.; Chen, L.; Lu, Y.; Su, Y. F.; Jia, Y. N.; Bao, L. Y.; Wang, J.; Chen, S.; Chen, R. J. Metal-organic frameworks composites threaded on the CNT knitted separator for suppressing the shuttle effect of lithium sulfur batteries. *Energy Storage Mater.* **2018**, *14*, 383−391.

(25) Maihom, T.; Sittiwong, J.; Probst, M.; Limtrakul, J. Understanding the interactions between lithium polysulfides and anchoring materials in advanced lithium-sulfur batteries using density functional theory. *Phys. Chem. Chem. Phys.* **2022**, *24*, 8604−8623.

(26) Park, H.; Siegel, D. J. Tuning the Adsorption of Polysulfides in Lithium-Sulfur Batteries with Metal-Organic Frameworks. *Chem. Mater.* **2017**, *29*, 4932−4939.

(27) Zhao, R.; Wu, Y.; Liang, Z.; Gao, L.; Xia, W.; Zhao, Y.; Zou, R. Metal−organic frameworks for solid-state electrolytes. *Energy Environ. Sci.* **2020**, *13*, 2386−2403.

(28) Shang, S. C.; Du, C. S.; Liu, Y. X.; Liu, M. H.; Wang, X. Y.; Gao, W. Q.; Zou, Y.; Dong, J. C.; Liu, Y. Q.; Chen, J. Y. A one-dimensional conductive metal-organic framework with extended conjugated nanoribbon layers. *Nat. Commun.* **2022**, *13*, 7599.
(29) Xie, L. S.; Skorupskii, G.; Dinca, M. Electrically Conductive Metal-Organic Frameworks. *Chem. Rev.* **2020**, *120*, 8536−8580.
(30) Zulueta, Y. A.; Nguyen, M. T. Theoretical approaches to defect mechanisms and transport properties of compounds used for electrodes and solid-state electrolytes in alkali-ion batteries. *Phys. Chem. Chem. Phys.* **2023**, *25*, 27926−27935.
(31) Rambabu, D.; Lakraychi, A. E.; Wang, J.; Sieuw, L.; Gupta, D.; Apostol, P.; Chanteux, G.; Goossens, T.; Robeyns, K.; Vlad, A. An Electrically Conducting Li-Ion Metal−Organic Framework. *J. Am. Chem. Soc.* **2021**, *143*, 11641−11650.
(32) Li, L.; Ji, C.; Wang, W.; Wu, F.; Tan, Y.-X.; Yuan, D. The effect of pore sizes on D2/H2 separation conducted by MOF-74 analogues. *Inorganic Chemistry Frontiers* **2022**, *9*, 1674−1680.
(33) Zheng, J. M.; Tian, J.; Wu, D. X.; Gu, M.; Xu, W.; Wang, C. M.; Gao, F.; Engelhard, M. H.; Zhang, J. G.; Liu, J.; et al. Lewis Acid-Base Interactions between Polysulfides and Metal Organic Framework in Lithium Sulfur Batteries. *Nano Lett.* **2014**, *14*, 2345−2352.
(34) Li, Y. X.; Zeng, Y. X.; Chen, Y.; Luan, D. Y.; Gao, S. Y.; Lou, X. W. Mesoporous N-rich Carbon with Single-Ni Atoms as a Multifunctional Sulfur Host for Li-S Batteries. *Angew. Chem., Int. Ed.* **2022**, *61*, No. e202212680.
(35) Hohenberg, P.; Kohn, W. Inhomogeneous Electron Gas. *Phys. Rev.* **1964**, *136*, B864−B871.
(36) Blöchl, P. E. Projector augmented-wave method. *Phys. Rev. B* **1994**, *50*, 17953−17979.
(37) Kresse, G.; Furthmüller, J. Efficient iterative schemes for ab initio total-energy calculations using a plane-wave basis set. *Phys. Rev. B* **1996**, *54*, 11169−11186.
(38) Lee, K.; Murray, É. D.; Kong, L.; Lundqvist, B. I.; Langreth, D. C. Higher-accuracy van der Waals density functional. *Phys. Rev. B* **2010**, *82*, No. 081101.
(39) Dion, M.; Rydberg, H.; Schröder, E.; Langreth, D. C.; Lundqvist, B. I. Van der Waals Density Functional for General Geometries. *Phys. Rev. Lett.* **2004**, *92*, No. 246401.
(40) Liechtenstein, A. I.; Anisimov, V. I.; Zaanen, J. Density-Functional Theory and Strong-Interactions - Orbital Ordering in Mott-Hubbard Insulators. *Phys. Rev. B* **1995**, *52*, R5467−R5470.
(41) Lin, K. Y.; Nachimuthu, S.; Huang, H. W.; Jiang, J. C. Theoretical insights on alleviating lattice-oxygen evolution by sulfur substitution in $Li_{1.2}Ni_{0.6}Mn_{0.2}O_2$ cathode material. *Npj Comput. Mater.* **2022**, *8*, 210.
(42) Nishihara, S.; Otani, M. Hybrid solvation models for bulk, interface, and membrane: Reference interaction site methods coupled with density functional theory. *Phys. Rev. B* **2017**, *96*, No. 115429.
(43) Haruyama, J.; Ikeshoji, T.; Otani, M. Electrode potential from density functional theory calculations combined with implicit solvation theory. *Phys. Rev. Mater.* **2018**, *2*, No. 095801.
(44) Giannozzi, P.; Baroni, S.; Bonini, N.; Calandra, M.; Car, R.; Cavazzoni, C.; Ceresoli, D.; Chiarotti, G. L.; Cococcioni, M.; Dabo, I.; et al. QUANTUM ESPRESSO: a modular and open-source software project for quantum simulations of materials. *J. Phys.: Condens. Matter* **2009**, *21*, No. 395502.
(45) Giannozzi, P.; Andreussi, O.; Brumme, T.; Bunau, O.; Buongiorno Nardelli, M.; Calandra, M.; Car, R.; Cavazzoni, C.; Ceresoli, D.; Cococcioni, M.; et al. Advanced capabilities for materials modelling with Quantum ESPRESSO. *J. Phys.: Condens. Matter* **2017**, *29*, No. 465901.
(46) Garrity, K. F.; Bennett, J. W.; Rabe, K. M.; Vanderbilt, D. Pseudopotentials for high-throughput DFT calculations. *Comput. Mater. Sci.* **2014**, *81*, 446−452.
(47) Laasonen, K.; Pasquarello, A.; Car, R.; Lee, C.; Vanderbilt, D. Car-Parrinello molecular dynamics with Vanderbilt ultrasoft pseudopotentials. *Phys. Rev. B* **1993**, *47*, 10142−10153.
(48) Jorgensen, W. L.; Tirado-Rives, J. The OPLS [optimized potentials for liquid simulations] potential functions for proteins, energy minimizations for crystals of cyclic peptides and crambin. *J. Am. Chem. Soc.* **1988**, *110*, 1657−1666.
(49) He, Q.; Yu, B.; Li, Z.; Zhao, Y. Density Functional Theory for Battery Materials. *Energy and Environmental Materials* **2019**, *2*, 264−279.
(50) Lo, W. T.; Yu, C.; Leggesse, E. G.; Nachimuthu, S.; Jiang, J. C. Understanding the Role of Dopant Metal Atoms on the Structural and Electronic Properties of Lithium-Rich $Li_{1.2}Ni_{0.2}Mn_{0.6}O_2$ Cathode Material for Lithium-Ion Batteries. *J. Phys. Chem. Lett.* **2019**, *10*, 4842−4850.
(51) Xu, B.; Fell, C. R.; Chi, M. F.; Meng, Y. S. Identifying surface structural changes in layered Li-excess nickel manganese oxides in high voltage lithium ion batteries: A joint experimental and theoretical study. *Energy Environ. Sci.* **2011**, *4*, 2223−2233.

https://doi.org/10.1021/acs.jpcc.4c03165
J. Phys. Chem. C 2024, 128, 16334−16342